JACS
JOURNAL OF THE AMERICAN CHEMICAL SOCIETY
Communication
pubs.acs.org/JACS

Direct Carbonization of Al-Based Porous Coordination Polymer for Synthesis of Nanoporous Carbon

Ming Hu,[†] Julien Reboul,[‡,§] Shuhei Furukawa,[‡,§] Nagy L. Torad,[†,∥] Qingmin Ji,[†] Pavuluri Srinivasu,[†] Katsuhiko Ariga,[†,⊥] Susumu Kitagawa,[‡,§] and Yusuke Yamauchi*[,†,∥,⊥]

[†]World Premier International (WPI) Research Center for Materials Nanoarchitectonics (MANA), National Institute for Materials Science (NIMS), 1-1 Namiki, Tsukuba, Ibaraki 305-0044, Japan

[‡]ERATO Kitagawa Integrated Pores Project, Japan Science and Technology Agency (JST), Kyoto Research Park Bldg #3, Shimogyo, Kyoto 600-8815, Japan

[§]Institute for Integrated Cell-Material Sciences (iCeMS), Kyoto University, Yoshida, Sakyo, Kyoto 606-8501, Japan

[∥]Faculty of Science and Engineering, Waseda University, 3-4-1 Okubo, Shinjuku, Tokyo 169-8555, Japan

[⊥]Core Research for Evolutional Science and Technology (CREST) & Precursory Research for Embryonic Science and Technology (PRESTO), Japan Science and Technology Agency (JST), 4-1-8, Honcho, Kawaguchi, Saitama 332-0012, Japan

Supporting Information

ABSTRACT: Nanoporous carbon (NPC) is prepared by direct carbonization of Al-based porous coordination polymers (Al-PCP). By applying the appropriate carbonization temperature, both high surface area and large pore volume are realized for the first time. Our NPC shows much higher porosity than other carbon materials (such as activated carbons and mesoporous carbons). This new type of carbon material exhibits superior sensing capabilities toward toxic aromatic substances.

Carbon materials, such as nanoporous carbon (NPC) (including mesoporous carbon)[1] and carbon nanotubes,[2] have been thoroughly studied to find practical applications. NPCs with high surfaces are especially promising. The unique nature of nanoporous structures permits their use in a variety of research, such as contamination removal, gas storage, supercapacitors, and carriers for drug delivery systems. For these applications, both high surface areas and large pore volumes are the most critical. To enhance these factors, many attempts have been made. For example, thermal decomposition of wood, coal, or organic materials; a template method; CVD; and laser ablation have been used to fabricate the nanostructured carbons.[3]

Ordered mesoporous carbons, which are promising as NPC materials, are generally prepared with a hard-templating method relying on mesoporous silicas. Hyeon et al. synthesized well-ordered mesoporous carbons by using mesoporous silicas as hard templates.[4] Ryoo et al. have reported mesoporous carbons (CMK family) by using mesoporous silicas, such as MCM-48, SBA-1, and SBA-15, as hard-templates.[5] Very recently, porous coordination polymers (PCPs) or metal–organic frameworks (MOFs), which are crystalline compounds consisting of metal ions coordinated to rigid organic molecules to form one-, two-, or three-dimensional structures,[6] have been demonstrated as novel templates to prepare microporous carbons.[7] By choosing suitable PCPs or MOFs with high thermal stability, the carbonization of carbon sources occurs inside the micropores, and the original porous structures of PCPs or MOFs are thus retained. For instance, when furfuryl alcohol is used as a carbon source, its molecular dimensions make it sufficient for entering and filling the framework of MOF-5 (zeolite-type MOF, ZIF-8)[7a,f] or Al-based PCP.[7e] After the carbonization of furfuryl alcohol, the resultant NPCs showed surface areas larger than 500 $m^2 \cdot g^{-1}$, even larger than 3000 $m^2 \cdot g^{-1}$. On the basis of such promising results, MOF- or PCP-templated carbonization deserves more attention.[7]

Here, we propose an alternative simple pathway for synthesis of NPC material. Considering the large carbon content of organic components in MOFs or PCPs, additional carbon sources as additives (e.g., furfuryl alcohol) are not always necessary. This idea provided the motivation to try a new system of "direct conversion of MOFs or PCPs." This process is a very simple, one-step pathway. Here, we selected a typical Al-based PCP (Al-PCP, $(Al(OH)(1,4\text{-NDC})\cdot 2H_2O)$[8] as an initial precursor. This Al-PCP was carbonized directly in an inert atmosphere. By changing the calcination temperatures, we investigated the changes of the surface areas. Surprisingly, the NPC treated at 800 °C showed very high surface area and large pore volume. Recently, several coordination polymers that exhibited large porosity have been demonstrated as a new category of porous materials. For example, Furukawa et al. reported a novel MOF having a high surface area of ∼6000 $m^2 \cdot g^{-1}$,[9a] and Ben et al. reported a porous polymer of ∼7000 $m^2 \cdot g^{-1}$.[9b] Compared to them, pure NPC materials are currently in high demand for sensing applications.

In the experiments, Al-PCP powders as the initial precursor were prepared according to a previous report.[8] Then, the Al-PCP powders were directly calcined in a furnace under protection of an inert gas. The applied calcination temperatures were varied from 500 to 800 °C. After the calcination, the obtained samples were washed extensively with an HF solution to remove the residual Al component. The obtained samples were designated as "PCP-*x*," where the "*x*" indicates the applied

Received: September 22, 2011
Published: January 24, 2012

dx.doi.org/10.1021/ja208940u | J. Am. Chem. Soc. 2012, 134, 2864–2867

calcination temperatures. Interestingly, the original fibrous shapes observed in the case of the Al-PCP precursor[8] were well retained in the final products (Figure 1).

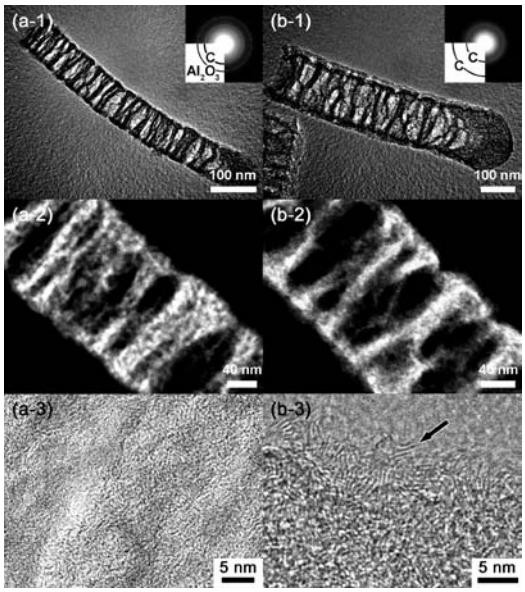

Figure 1. Bright- and dark-field TEM images of Al-PCP calcined at 800 °C (a) before and (b) after washing with HF. The inset is the corresponding ED pattern. (a-3, b-3) High resolution TEM images of Al-PCP calcined at 800 °C before and after washing by HF, respectively. The graphitic sheets are indicated by arrow.

Wide-angle X-ray diffraction was performed on all the samples (Figure S1a–d). Several broad peaks, belonging to a typical (002) interlayer peak of graphitic carbon, were observed at 2θ = 25° and 44°. However, we did not see an in-plane structural sign of typical graphitic carbon at around 2θ = 13°, indicating that the graphitic structures were not well developed in the products. PCP-800 before HF treatment showed a small peak assignable to alumina (JCPDS 88-1609) (Figure S1e). The alumina was formed by a dehydration reaction of Al(OH) parts of Al-PCP under high temperature. After HF treatment, the alumina was totally removed. To further check the compositions of the samples after HF treatment, elemental analysis (carbon, hydrogen, and nitrogen) was performed. The results confirmed that the main composition was carbon (~85 wt %) together with trace amounts of nitrogen (~1.0 wt %). Oxygen (~10 wt %) and hydrogen (~4.0 wt %) were also detected, likely due to the oxygen-containing carbon network, hydroxyl groups, and adsorbed water molecules.[10] On the basis of both the XRD patterns and the elemental analysis results, carbon was successfully obtained through the thermal decomposition of Al-PCPs, and the other inorganic elements, such as Al, could be completely removed using HF.

Raman spectra for all the samples are shown in Figure S2. All the spectra exhibited *D* and *G* bands at 1345 and 1588 cm^{-1}, respectively. In general, the appearance of the *D* peak is associated with the presence of a disordered carbon structure. In addition, as the number of defects increases, the intensity of the *D* band increases. In the case of carbon nanotubes (single-wall carbon nanotube) and pure graphitic carbon, the *D* peaks are not observable, and only *G* peaks appear. The relative ratios of the *G* bands to the *D* bands (I_G/I_D) illustrate the crystallization degree of graphitic carbon. On the basis of the Raman spectra shown in Figure S2, the relative ratios of the *G* bands are almost constant, irrespective of the applied calcination temperatures. These values are almost the same as those of active carbon. The appearance of the obvious *D* peaks in all the samples indicated that, unlike graphite, graphene sheets were not developed in the products. In fact, high-resolution TEM images (Figure 1b-3) reveal the obtained carbon materials were made up by randomly assembling the nanometer-sized sheets, which coincided with the Raman and XRD results (TEM data details are given in a later section).

To observe the morphology, SEM images were taken from all the samples (Figure S3). Compared to initial Al-PCP,[8] the obtained carbon materials had a similar fiber-like morphology. It is noteworthy that such a fiber-like morphology was retained even after HF treatment. In some parts, large cracks/voids were formed after the calcination followed by HF treatment, which was most likely caused by the large weight loss during thermal decomposition of organic components of the Al-PCPs. Compared to the initial Al-PCP weight before the calcination, an ~60–70 wt % weight loss was confirmed by the calcination process (from 500 to 800 °C), as confirmed by TG data (Figure S4). When the applied calcination temperature was 500 °C, the fibrous shape slightly collapsed by HF treatment, which was caused by insufficient carbonization of the carbon. By increasing the applied calcination temperatures, condensed carbonized networks with more chemical stability were formed. Therefore, the original fibrous shapes were well retained.

To characterize the detailed microstructure of the obtained NPC, PCP-800 samples before and after HF treatment were carefully observed by TEM. Bright-field TEM images (Figure 1) showed both samples possessed nanoporous structures. Large cracks/voids were observed and confirmed by SEM observation (Figure S3). In a sense, a hierarchical porous structure was realized here. In both samples, selected-area electron diffraction (ED) patterns presented a weak ring-like pattern derived from typical amorphous carbon. From a high-resolution TEM image, we observed that a few carbon layers were randomly aggregated inside the fibers. Before HF treatment, a very weak ring could be assigned to a (220) peak of the alumina phase. However, after HF treatment, no Al content was confirmed by elemental analysis.

For all the samples (PCP-500, PCP-600, PCP-700, and PCP-800), their specific surface areas and pore-size distribution were characterized by using N_2 adsorption–desorption isotherms (Table S1). At low relative pressure area (P/P_0 < 0.1), the isotherms showed a drastic uptake at very low P/P_0, indicating the presence of micropores (Figure 2a). The pore-size distribution calculated using a method called Non-Localized Density Functional Theory (NLDFT) was widely distributed from 1 to 5 nm (Figure S5a). Specific surface areas and pore volumes were calculated by BET and *t*-plot methods, respectively (Figure 2b). After removing the Al species by HF treatment, the surface areas were further increased. In particular, in the case of PCP-800, the amounts of adsorbed nitrogen increased drastically in the range of P/P_0 = 0.05–0.3, showing an extremely high surface area (5500 $m^2 \cdot g^{-1}$). To confirm reproducibility, we prepared 10 samples under the same conditions and then used their average surface areas for Figure 2b. The average pore volume in PCP-800 was calculated to be 4.3 $cc \cdot g^{-1}$ by the *t*-plot method, which was also confirmed by NLDFT (4.4 $cc \cdot g^{-1}$) (Figure S5b). When Al-PCP was calcined at higher temperatures (over 900 °C), the surface areas decreased drastically to ~200 $m^2 \cdot g^{-1}$ due to the collapse of the

dx.doi.org/10.1021/ja208940u | J. Am. Chem. Soc. 2012, 134, 2864–2867

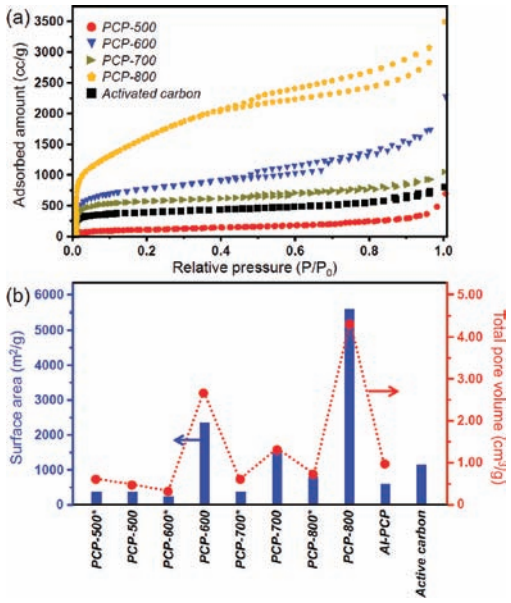

Figure 2. (a) N_2 adsorption−desorption isotherms for the obtained samples calcined at various temperatures (PCP-500, PCP-600, PCP-700, and PCP-800). The isotherm for active carbon is also shown as a reference. (b) Summary of surface areas and total pore volumes for the obtained samples. For comparison, the samples before HF treatment are also shown, as indicated by (*). The exact values are given in Table S1.

nanoporous structure caused by graphitization. In such a case, additional carbon sources as additives (e.g., furfuryl alcohol) are necessary for the retention of porous structure.[7]

The surface area obtained here exceeds that of commercially available active carbons (as shown in Figure 2a, surface area = 1142 $m^2 \cdot g^{-1}$) and single-wall carbon nanotubes (at most 2500 $m^2 \cdot g^{-1}$), to the best of our knowledge. To date, many attempts have been made to prepare NPC materials with high surface areas. Kyotani et al. have reported ordered microporous carbon synthesized in the confined space of zeolite nanochannels, realizing surface areas of ~4000 $m^2 \cdot g^{-1}$.[11] Hyeon et al. and Ryoo et al. have reported various types of mesoporous carbons.[4,5] Although the surface areas can be controlled by the selection of original mesoporous silica templates and carbon sources, the surface areas of mesoporous carbons are limited to less than 2000 $m^2 \cdot g^{-1}$.[4,5,12] The above replication processes are complex because the synthetic pathway involves several steps: (i) formation of the original templates, (ii) filling the carbon precursors into mesopores, (iii) converting the precursors into solids, and (iv) removal of the original templates. In contrast, our new system, "direct conversion of MOFs or PCPs," is a really simple pathway.

To investigate the mechanical stability of PCP-800, we checked the change in surface area by applying a mechanical pressure treatment (10 MPa for 10 min). After the treatment, the loss of surface area and pore volume was calculated to be ~35%. Our NPC could still work under such high pressure, although the performance could not be as good as that under mild conditions.

Encouraged by the high surface area and large pore volume, we examined the sensing capabilities for toxic aromatic substances using a quartz crystal microbalance (QCM) technique. Currently, molecular sensing of toxic substances has been extensively investigated and has revealed that well-designed host structures are essential for high sensitivities as well as of fundamental importance in chemical sensing applications.[13] For this purpose, we designed a QCM sensor by mixing PCP-800 powder with polyelectrolyte binders. For comparison, commercially available active carbon (shown in Figure 2) was also introduced. The same amounts of sample (20 $\mu g \cdot cm^{-2}$) were deposited onto the QCM electrode. Then, the designed QCM sensor with PCP-800 was exposed to vaporized gas, and the time dependence of the frequency shifts (Δf) was plotted (Figure 3a). The sensing of benzene vapors

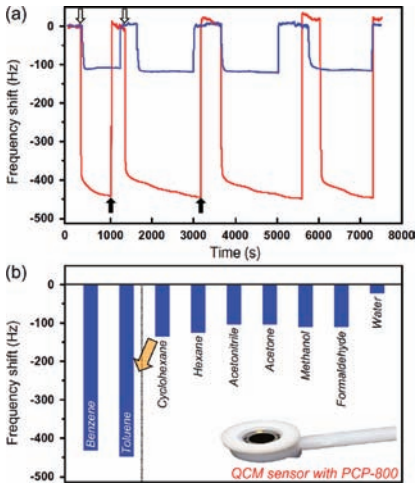

Figure 3. (a) QCM frequency shifts upon benzene adsorption into (red line) PCP-800 film and (blue line) active carbon film. Changes in QCM frequency shifts are examined through alternate exposure (open arrows) and removal (filled arrows) of the benzene molecules. (b) Summary of QCM frequency shifts of PCP-800 film caused by exposure to various vaporized gases. These QCM frequency shifts are recorded 500 s after the PCP-800 films are exposed to vapors.

can be repeated well through alternate exposure and removal of the benzene molecules (Figure 3a). In the case of PCP-800, we clearly observed large adsorption uptake for benzene vapors. The response was very fast, and the frequency was immediately changed (Δf = 392 Hz) after a few seconds. Compared to active carbon, PCP-800 provided almost 4 times higher uptakes for benzene vapors. The large difference in adsorption capacity was caused by the very high porosity.

In contrast, our QCM sensor coated with PCP-800 showed very small adsorption uptakes for cyclohexane and hexane vapors. Their frequency shifts (Δf) were 141 Hz (for cyclohexane) and 130 Hz (for hexane), respectively. The sensing activity of benzene is approximately three times higher than that of cyclohexane and hexane, although the three have similar molecular sizes and molecular weights (Figure 3b). The graphitic carbon containing sp^2-hybridized carbons (observed in Figure 1b-3) has a higher affinity for aromatic hydrocarbons than for their aliphatic analogues.[13d,e] As clearly indicated in Figure 3b, our QCM sensor has superior affinity for aromatic compounds than for aliphatic compounds, which is very important for the highly selective detection of aromatic substances. The vaporized aromatic hydrocarbons can freely diffuse inside the pores with $\pi-\pi$ interaction between benzene molecules and graphitic carbon frameworks. Toluene is also a very toxic aromatic substance to humans. Superior sensing capabilities for toluene vapor could also be realized by both enhancement of host−guest interaction and an increase of the

dx.doi.org/10.1021/ja208940u | J. Am. Chem. Soc. 2012, 134, 2864−2867

surface area. When PCP-800 was exposed to toluene vapors, a drastic decrease in the frequency of QCM was observed due to the large adsorption uptake for toluene molecules (Figure S6). The frequency shift (Δf) was 438 Hz, which was almost two times higher than that of active carbon. It has been generally known that an amorphous carbon contains both sp^2- and sp^3-hybridized carbons. The sp^2/sp^3 ratio can be roughly estimated by using Raman spectroscopy.[14] Figure S2 shows that both PCP-800 and active carbon have G peaks at ~1589 cm^{-1} and their I_G/I_D ratio is almost the same, indicating that the sp^2/sp^3 ratios in both samples were very similar. Therefore, it was concluded that the large differences in adsorption capacity were caused by the surface areas. From theoretical calculation (see Figure S7), it was further demonstrated that toluene adsorption into PCP-800 proceeded more rapidly than that in active carbon.

In conclusion, we successfully prepared NPC with a high surface area and large pore volume by the simple thermal decomposition of Al-PCPs. By using this novel carbon material, we realized a large uptake of aromatic compounds within a very short time. These findings are a striking indication toward the highly selective detection of aromatic guests. Through this report, we demonstrated that Al-PCP was a very promising precursor for preparing NPCs with advanced functions.

■ ASSOCIATED CONTENT

Ⓢ Supporting Information

Experimental details and other characterization data for nanoporous carbon materials. This material is available free of charge via the Internet at http://pubs.acs.org.

■ AUTHOR INFORMATION

Corresponding Author

Yamauchi.Yusuke@nims.go.jp

Notes

The authors declare no competing financial interest.

■ REFERENCES

(1) (a) Lee, J.; Kim, J.; Hyeon, T. *Adv. Mater.* **2006**, *18*, 2073. (b) Ariga, K.; Hill, J. P.; Lee, M. V.; Vinu, A.; Charvet, R.; Acharya, S. *Sci. Technol. Adv. Mater.* **2008**, *9*, 014109. (c) Liang, C.; Li, Z.; Dai, S. *Angew. Chem., Int. Ed.* **2008**, *47*, 3696. (d) Kim, J. H.; Yu, J. S. *Phys. Chem. Chem. Phys.* **2010**, *12*, 15301. (e) Fang, B.; Kim, J. H.; Lime, S.; Yu, J. S. *J. Mater. Chem.* **2010**, *20*, 10253. (f) Kim, J. H.; Fang, B.; Kim, M. S.; Yoon, S. B.; Bae, T. S.; Ranade, D. R.; Yu, J. S. *Electrochim. Acta* **2010**, *55*, 7628. (g) Fang, Y.; Gu, D.; Zou, Y.; Wu, Z.; Li, F.; Che, R.; Deng, Y.; Tu, B.; Zhao, D. *Angew. Chem., Int. Ed.* **2010**, *49*, 7987. (h) Lv, Y.; Liu, M.; Gan, L.; Cao, Y. J.; Chen, L.; Xiong, W.; Xu, Z.; Hao, Z.; Liu, H.; Chen, L. *Chem. Lett.* **2011**, *40*, 236.

(2) (a) Murakami, Y.; Chiashi, S.; Miyauchi, Y.; Hu, M.; Ogura, M.; Okubo, T.; Maruyama, S. *Chem. Phys. Lett.* **2004**, *385*, 298. (b) Piao, Y.; An, K.; Kim, J.; Yu, T.; Hyeon, T. *J. Mater. Chem.* **2006**, *16*, 2984. (c) Kim, M. S.; Lim, S.; Song, M. Y.; Cho, H.; Choi, Y.; Yu, J. S. *Carbon Lett.* **2010**, *11*, 336. (d) Ozawa, H.; Ide, N.; Fujigaya, T.; Niidome, Y.; Nakashima, N. *Chem. Lett.* **2011**, *40*, 239. (e) Piao, Y.; Jin, Z.; Lee, D.; Lee, H. J.; Na, H. B.; Hyeon, T.; Oh, M. K.; Kim, J.; Kim, H. S. *Biosens. Bioelectron.* **2011**, *26*, 3192.

(3) (a) Liu, J.; Qiao, S. Z.; Liu, H.; Chen, J.; Orpe, A.; Zhao, D.; Lu, G. Q. *Angew. Chem., Int. Ed.* **2011**, *50*, 5947. (b) Liang, C.; Dai, S. *Chem. Mater.* **2009**, *21*, 2115. (c) Shang, N.; Papakonstantinou, P.; Wang, P.; Zakharov, A.; Palnitkar, U.; Lin, I. N.; Chu, M.; Stamboulis, A. *ACS Nano* **2009**, *3*, 1032. (d) Chun, H.; Hahm, M. G.; Homma, Y.; Meritz, R.; Kuramochi, K.; Menon, L.; Ci, L.; Ajayan, P. M.; Jung, Y. J. *ACS Nano* **2009**, *3*, 1274. (e) Thess, A; Lee, R.; Nikolaev, P.; Dai, H.; Petit, P.; Robert, J.; Xu, C.; Lee, Y. H.; Kim, S. G.; Rinzler, A. G.; Colbert, D. T.; Scuseria, G. E.; Tománek, D.; Fischer, J. E.; Smalley, R. E. *Science* **1996**, *273*, 483.

(4) (a) Lee, J.; Yoon, S.; Hyeon, T.; Oh, S. M.; Kim, K. B. *Chem. Commun.* **1999**, 2177. (b) Lee, J.; Yoon, S.; Oh, S. M.; Shin, C. H.; Hyeon, T. *Adv. Mater.* **2000**, *12*, 359. (c) Yoon, S.; Lee, J.; Hyeon, T.; Oh, S. M. *J. Electrochem. Soc.* **2000**, *147*, 2507. (d) Lee, J.; Kim, J.; Hyeon, T. *Chem. Commun.* **2003**, 1138.

(5) (a) Ryoo, R.; Joo, S. H.; Jun, S. *J. Phys. Chem. B* **1999**, *103*, 7743. (b) Jun, S.; Joo, S. H.; Ryoo, R.; Kruk, M.; Jaroniec, M; Liu, Z.; Ohsuna, T.; Terasaki, O. *J. Am. Chem. Soc.* **2000**, *122*, 10712.

(6) (a) Férey, G.; Latroche, M.; Serre, C.; Milange, F.; Loiseau, T.; Percheron-Guégan, A. *Chem. Commun.* **2003**, 2976. (b) Rosi, N. L.; Eckert, J.; Eddaoudi, M.; Vodak, D. T.; Kim, J.; O'Keeffe, M.; Yaghi, O. M. *Science* **2003**, *300*, 1127. (c) Wang, B.; Côté, A. P.; Furukawa, H.; O'Keeffe, M.; Yaghi, O. M. *Nature* **2008**, *453*, 207. (d) Xiang, S.; Zhou, W.; Gallegos, J. M.; Liu, Y.; Chen, B. *J. Am. Chem. Soc.* **2009**, *131*, 12415. (e) Yang, R.; Li, L.; Xiong, Y.; Li, J. R.; Zhou, H. C.; Su, C. Y. *Chem. Asian J.* **2010**, *5*, 2358. (f) Ma, S.; Zhou, H. C. *Chem. Commun.* **2010**, *46*, 44. (g) Xiang, S.; Zhou, W.; Zhang, Z.; Green, M. A.; Liu, Y.; Chen, B. *Angew. Chem., Int. Ed.* **2010**, *49*, 4615. (h) Chen, B.; Xiang, S.; Qian, G. *Acc. Chem. Res.* **2010**, *43*, 1115. (i) Makal, T. A.; Yakovenko, A. A.; Zhou, H. C. *J. Phys. Chem. Lett.* **2011**, *2*, 1682. (j) Yuan, D.; Zhao, D.; Timmons, D. J.; Zhou, H. C. *Chem. Sci.* **2011**, *2*, 103. (k) Guo, Z.; Wu, H.; Srinivas, G.; Zhou, Y.; Xiang, S.; Chen, Z.; Yang, Y.; Zhou, W.; O'Keeffe, M.; Chen, B. *Angew. Chem., Int. Ed.* **2011**, *50*, 3178.

(7) (a) Liu, B.; Shioyama, H.; Akita, T.; Xu, Q. *J. Am. Chem. Soc.* **2008**, *130*, 5390. (b) Yuan, D.; Chen, J.; Tan, S.; Xia, N.; Liu, Y. *Electrochem. Commun.* **2009**, *11*, 1191. (c) Liu, B.; Shioyama, H.; Jiang, H. L.; Zhang, X. B.; Xu, Q. *Carbon* **2010**, *48*, 456. (d) Hu, J.; Wang, H.; Gao, Q.; Guo, H. *Carbon* **2010**, *48*, 3599. (e) Radhakrishnan, L.; Reboul, J.; Furukawa, S.; Srinivasu, P.; Kitagawa, S.; Yamauchi, Y. *Chem. Mater.* **2011**, *23*, 1225. (f) Jiang, H. L.; Liu, B.; Lan, Y. Q.; Kuratani, K.; Akita, T.; Shioyama, H.; Zong, F.; Xu, Q. *J. Am. Chem. Soc.* **2011**, *133*, 11854.

(8) Comotti, A.; Bracco, S.; Sozzani, P.; Horike, S.; Matsuda, R.; Chen, J.; Takata, M.; Kubota, Y.; Kitagawa, S. *J. Am. Chem. Soc.* **2008**, *130*, 13664.

(9) (a) Furukawa, H.; Ko, N.; Go, Y. B.; Aratani, N.; Choi, S. B.; Choi, E.; Yazaydin, A. Ö.; Snurr, R. Q.; O'Keeffe, M.; Kim, J.; Yaghi, O. M. *Science* **2010**, *329*, 424. (b) Ben, T.; Ren, H.; Ma, S.; Cao, D.; Lan, J.; Jing, X.; Wang, W.; Xu, J.; Deng, F.; Simmons, J. M.; Qiu, S.; Zhu, G. *Angew. Chem., Int. Ed.* **2009**, *48*, 9457.

(10) Nishihara, H.; Yang, Q. H.; Hou, P. X.; Unno, M.; Yamauchi, S.; Saito, R.; Paredes, J. I.; Martínez-Alonso, A.; Tascón, J. M. D.; Sato, Y.; Terauchi, M.; Kyotani, T. *Carbon* **2009**, *47*, 1220.

(11) (a) Kyotani, T.; Nagai, T.; Inoue, S.; Tomita, A. *Chem. Mater.* **1997**, *9*, 609. (b) Rodriguez-Mirasol, J.; Cordero, T.; Radovic, L. R.; Rodriguez, J. J. *Chem. Mater.* **1998**, *10*, 550. (c) Ma, Z.; Kyotani, T.; Tomita, A. *Chem. Commun.* **2000**, 2365. (d) Ma, Z.; Kyotani, T.; Liu, Z.; Terasaki, O.; Tomita, A. *Chem. Mater.* **2001**, *13*, 4413.

(12) (a) Che, S.; Garcia-Bennett, A. E.; Liu, X.; Hodgkins, R. P.; Wright, P. A.; Zhao, D.; Terasaki, O.; Tatsumi, T. *Angew. Chem., Int. Ed.* **2003**, *42*, 3930. (b) Li, H.; Sakamoto, Y.; Li, Y.; Terasaki, O.; Thommes, M.; Che, S. *Microporous Mesoporous Mater.* **2006**, *95*, 193.

(13) (a) Müller, E. A.; Rull, L. F.; Vega, L. F.; Gubbins, K. E. *J. Phys. Chem.* **1996**, *100*, 1189. (b) Rutherford, S. W. *Langmuir* **2006**, *22*, 702. (c) Park, J. I.; Yu, I.; Seo, Y. *J. Appl. Phys.* **2007**, *101*, 053521. (d) Ariga, K.; Vinu, A.; Ji, Q.; Ohmori, O.; Hill, J. P.; Acharya, S.; Koike, J.; Shiratori, S. *Angew. Chem., Int. Ed.* **2008**, *47*, 7254. (e) Ji, Q.; Honma, I.; Paek, S. M.; Akada, M.; Hill, J. P.; Vinu, A.; Ariga, K. *Angew. Chem., Int. Ed.* **2010**, *49*, 9737.

(14) Ferrari, A. C.; Robertson, J. *Phys. Rev. B* **2000**, *61*, 14095.